# Compatibilizing Poly(vinylidene fluoride)/Nylon-6 Blends with Nanoclay

**Loan T. Vo and Emmanuel P. Giannelis***

*Department of Materials Science and Engineering, Cornell University, Bard Hall, Ithaca, New York 14853*

*Received July 8, 2007; Revised Manuscript Received August 21, 2007*

ABSTRACT: Blends of poly(vinylidene fluoride)/nylon-6 (PVDF/N6) 30:70 were melt compounded with various organoclays directly or sequentially. The morphology, thermal, and mechanical properties of the blend nanocomposites were investigated. It was determined that the degree of compatibilization induced by the nanoclay particles was dependent on the location of the particles and the degree of clay dispersion. The blend nanocomposite with the best mechanical properties had good dispersion of particles throughout the matrix (N6) and at the PVDF/N6 interface. In this blend nanocomposite, the coalescence of PVDF domains was prevented, and the crystallization of the PVDF domains was suppressed, ultimately creating a blend nanocomposite that is stiffer, stronger, and tougher than the blend without nanoparticles.

## Introduction

Poly(vinylidene fluoride) (PVDF) is a semicrystalline engineering polymer with very good resistance to chemicals, oxidation, and UV radiation. However, it suffers from low strength and ductility. Nylon-6 (N6), another semicrystalline engineering thermoplastic, is very ductile and has good mechanical properties, but it is prone to water absorption and has poor resistance to thermal oxidation and UV radiation. An intuitive way to optimize the properties of these two polymers is to blend them. To that end, Liu et al. have studied PVDF/N6 blends of different compositions and have found that the polymers can have favorable molecular interactions compared to other immiscible polymer blends.[1] Despite the interaction though, PVDF/N6 blends are immiscible over the entire concentration range. To change the interface and improve the miscibility, researchers have attempted several methods of compatibilization including grafting a copolymer onto N6 which is compatible with PVDF[2] and complexation of N6 amide groups with zinc cations grafted onto PVDF.[3]

In this study, we use inorganic nanoparticles as an alternative means to control interfacial properties. Nanoclays are an attractive alternative to traditional compatibilizers because they can be inexpensive, easily melt compounded with polymers, and non-polymer specific potentially compatibilizing many different polymer blends. Nanoclays have also been shown to enhance the mechanical and thermal properties and stabilize different crystalline phases of a polymer.[4,5]

A few polymer blend/clay nanocomposite systems have already been studied.[6−15] Some of these systems exhibit finer morphology and improved interfacial adhesion.[6−9] Unfortunately, the polymer blend nanocomposites share the same tradeoffs as traditional polymer composites and some polymer nanocomposites: while the composites become stiffer, they also become less tough.[6,7] We report here a polymer blend/clay system with increases in stiffness, strength, and toughness. Furthermore, our studies using different clays as well as sequential compounding (i.e., incorporating the clay into one polymer before blending with the second polymer) reveal a trend that suggests toughness is related to the domain size and degree of crystallinity of the domain phase. The domain size is controlled by the PVDF/N6 viscosity ratio and interfacial tension which are ultimately determined from the surface modification of the nanoclay and the dispersion of the nanoclay particles.

## Experimental Part

N6 (1022B) pellets were provided by UBE Industries, ground to 2 mm particles, and dried at 80 °C under vacuum for 12 h. PVDF (Kynar 721) was provided by Arkema, and modified montmorillonite clays (Cloisite 30B and Cloisite 20A) were obtained from Southern Clay Products. Both were used as received. For the one batch samples, PVDF/N6 powders were combined in a 30:70 ratio with the appropriate amount of clay in a speed mixer. The mixture was extruded at 240 °C under flowing nitrogen for 5 min using a DSM twin-screw microcompounder. For the sequential studies, clay was first extruded with one polymer. The resulting composite was then ground to 2 mm particles and extruded with the second polymer of the blend. The amount of clay in the sequence blends was 4.76 wt % (PVDF/N6/clay 30:70:5) after blending. When studying blends with different clays, the wt % of silicate in the blends was held constant (3.3%). To mold dog-bone-shaped samples (ISO 527-2-5A standard) for tensile testing, a microinjector was used with the barrel at 275 °C , the mold at 110 °C , and the injection pressure at 110 psi.

Blend morphology was examined using a Leo 1550 Keck Field Emission SEM and a Technai T12 TEM operating at an accelerating voltage of 120 kV. Samples for the SEM were fractured under liquid nitrogen and then coated with Au/Pd. Samples for TEM were sectioned from molded dog bones to 70 nm at −60 °C using a diamond knife. The difference in electron density between N6 and PVDF was sufficient to provide contrast in the TEM. Domain size was determined using ImageJ processing program on several images ranging from 20K× to 50K× magnification. Diffraction spectra were collected on a Scintag Inc. $\theta-\theta$ diffractometer with a Cu K$\alpha$ source ($\lambda$ = 1.54 Å) and a germanium detector, scanning at 3° min$^{-1}$. The degree of crystallinity was evaluated by following the equations outlined previously[4,16] and using a TA Instruments Q1000 DSC scanning 10 °C/min from ambient temperature to 250 °C; a heat/cool/heat cycle was used to eliminate any thermal history in the extruded material. Thermomechanical properties were obtained from a TA Instruments DMA 2980 scanning from −70 to 200 °C operating at 1 Hz. Mechanical properties were determined using an Instron 5569 tensile tester at an extension rate of 5 mm/min (strain rate of 18%/min). Five dog bone specimens were tested for each sample. The standard deviations were within 10% of the

* Corresponding author. E-mail: epg2@cornell.edu.

10.1021/ma071508q CCC: $37.00 
Published on Web 10/04/2007

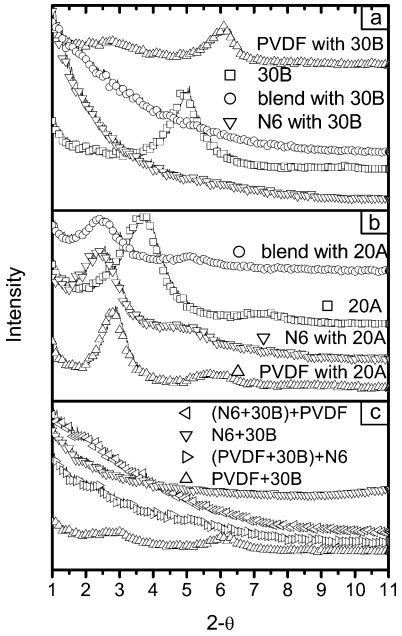


**Figure 1.** XRD plots for (a) 30B, PVDF with 5% 30B, N6 with 5% 30B, and PVDF:N6 30:70 blend with 5% 30B; (b) 20A, PVDF with 5% 20A, N6 with 5% 20A, and PVDF:N6 30:70 blend with 5% 20A; (c) composites after first step in sequential blending [PVDF with 14.3% 30B and N6 with 6.7% 30B] and after second step [(PVDF/30B)/N6 and (N6/30B)/PVDF)].

average values of the tensile properties. Rheological measurements were made using a MCR 300 under nitrogen flow at 240 °C in oscillatory shear configuration with a 1% strain.

## Results

**Homopolymers with Clay.** To aid determining the role of the clays in the blend, the effect of the clays on each polymer must be first ascertained. The clay nanoparticles used in this work were modified via cation exchange with quaternary ammonium cations to render the clay surface more organophilic. The differences in the functional groups of the cations offer varying affinities to the polymers such that the location of the clay can be tuned to optimize blend properties. Cloisite 30B (herein referred to as 30B) is modified with bis(2-hydroxyethyl) tallow alkylammonium and interacts more favorably with the polar amide group of N6. In N6, the clay is well dispersed (exfoliated), whereas it is intercalated in PVDF (Figure 1a). Cloisite 20A (herein referred to as 20A), modified with dimethyl dehydrogenated tallow alkylammonium, is less polar than 30B and interacts comparably with the two polymers; both PVDF and N6 intercalate 20A (Figure 1b). Given that N6 disperses one of the clays, N6 was chosen to be the matrix phase (70%) and PVDF to be the domain phase (30%).

**One Batch Blend with Cloisite 30B.** As expected from the known immiscibility of PVDF and N6, PVDF forms domains in the N6 matrix. The size of the largest domains is ~150 nm as determined from TEM and SEM imaging (Figure 2a,c). (In the TEM micrograph, dark zones represent PVDF domains.) In comparison, the morphology of the blend with 5% 30B clay is finer and more uniform with the largest domains being 60 nm (Figure 2b). The location of the clay nanoparticles was also investigated by TEM and SEM (Figure 2b,d). The TEM micrograph (Figure 2b) shows the majority of the clay dispersed in the N6 matrix. XRD patterns (Figure 1a) confirm the disordered (exfoliated) structure as the nanocomposite blend did not possess a characteristic peak indicative of layered clays. The TEM micrograph also shows some of the clay at the PVDF/N6 interface. The SEM micrograph of the fracture surface of this blend nanocomposite (Figure 2d) supports the improvement in the interfacial adhesion as the blend nanocomposite has fewer visible domains compared to the blend and shows practically no debonding.

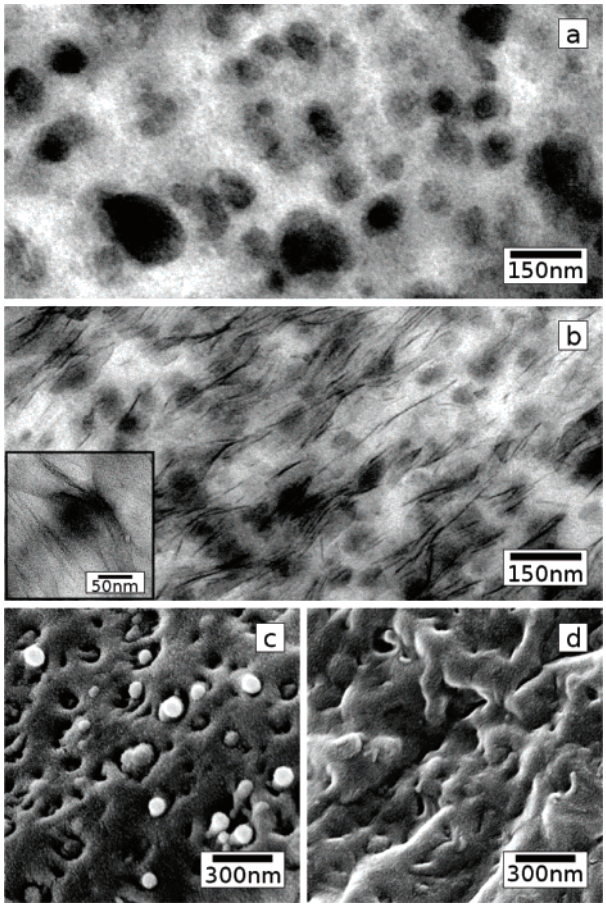


**Figure 2.** TEM micrographs of (a) PVDF/N6 30:70 blend and (b) 30:70 blend with 5% 30B. SEM micrographs of fracture surfaces of (c) PVDF/N6 30:70 blend and (d) blend with 5% 30B. Inset in (b) shows some clay residing the PVDF/N6 interface.

The presence of clay simultaneously in the bulk and the interface is atypical. Previous studies of polymer blend/clay systems usually show the clay residing either at the interface[6,9,13] or in the bulk.[7,10] This dual positioning indicates two roles for the nanoclay particles: one as a compatibilizer with the clay being shared by both polymers and the other as a nanofiller, stabilizing a different polymer crystalline phase and improving the mechanical properties as will be discussed in the following paragraphs.

Since 30B interacts favorably with N6, it is expected that the polymer would display the same polymorphism behavior as previously observed in nylon nanocomposites.[5,16,17] N6 has two stable crystalline phases, $\alpha$ and $\gamma$. Injection-molded N6 consists of a mixture of $\alpha$ and $\gamma$ phases, but upon clay addition N6 preferentially forms the $\gamma$ phase. From the wide-angle XRD patterns (Figure 3) and DSC melting thermographs of the blends (Figure 4a), N6 in the blends experiences the same crystal phase transformation when compounded with clay. In the blend with no clay, N6 exists mainly in the $\alpha$-form, but with increasing clay concentration, the ratio of $\alpha$ to $\gamma$ phase decreases with the 5% clay blend consisting mainly of $\gamma$ phase. (In Figure 3, the diffraction peaks at $2\theta = 19.5°$ and 23.5° correspond to the $\alpha$-phase while that at $2\theta = 21°$ corresponds to the $\gamma$-phase. In Figure 4a, the $\alpha$-form of N6 melts at 220 °C while the $\gamma$-form

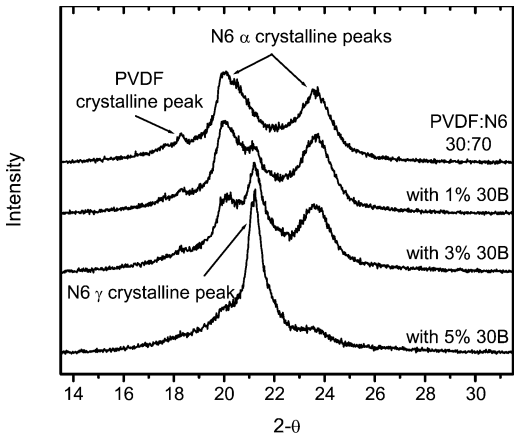


**Figure 3.** WAXS plots of the PVDF/N6 30:70 blend and blends with various concentrations of 30B.

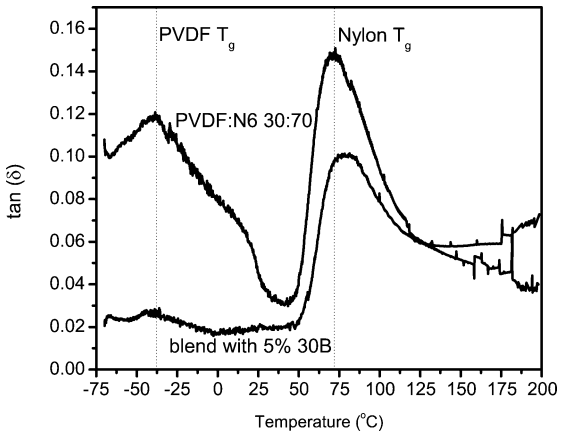


**Figure 5.** DMA tan $\delta$ curves showing the glass transition temperatures of PVDF and N6 for the blend and blend with 30B clay.

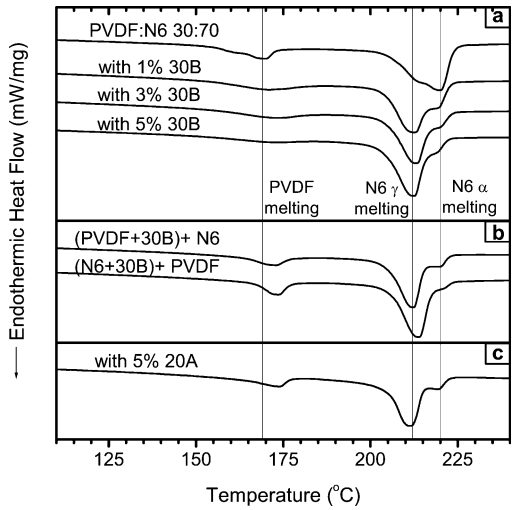


**Figure 4.** DSC melting curves for (a) PVDF/N6 30:70 blend and blends with various concentrations of 30B, (b) sequential 30B blends, and (c) one batch 20A blend.

melts at 212 °C.) In the blend nanocomposite, the clay in the N6 matrix acts as a nucleating agent stabilizing the $\gamma$ crystalline form of N6 similarly to the clay in the homopolymer.[16]

The effect of the clay on PVDF, however, is to hinder crystallization. The PVDF melting peak (at 169 °C) shifts to higher temperatures (indicating interaction with clay[4,18]) and decreases in area as the amount of clay increases (Figure 4a). In addition, the $T_c$ and $T_g$ peaks of PVDF are also suppressed as observed by DSC (not shown) and DMA (Figure 5), respectively. The crystallization and glass transition suppression are due to the restricted movement of the PVDF. Not only is the PVDF in smaller domains (such that the PVDF properties are no longer dominated by the larger more bulklike domains), but the PVDF chains are constrained by clay platelets surrounding the domains. Other studies with confined polymers have also shown suppressed thermal transitions.[14,19−22] For example, Nakajima et al.[19] found that polypropylene confined in mesoporous silica does not exhibit a crystalline melting point, and Jiang et al.[20] saw the same with poly(ethylene oxide) confined in organic networks.

One of the ultimate purposes for polymer blending and compatibilizing is to improve mechanical properties. If in fact there is compatibilization, the blend should exhibit improved mechanical properties. Figure 6a shows a representative stress/strain curve for the blend and the blend with 1 and 5% clay. With as little as 1% clay, the tensile properties of the blend nanocomposite are improved compared to the blend without clay. The blend with 5% clay is even stronger and tougher. Not only are the blend nanocomposites stiffer (with a modulus of $E = 2.68 \pm 0.05$ GPa for the 5% blend compared to $1.90 \pm 0.04$ GPa for the blend without clay), they also show higher elongation and strength. For the 5% clay blend, these improvements translate to ≈170% increase in toughness (defined as the area under a stress/strain plot). For comparison, the stress−strain curves of the homopolymers and their nanocomposites are shown in Figure 6b. The 30B blend nanocomposite also has higher yield and ultimate stresses and is stiffer than PVDF ($E = 1.31 \pm 0.06$ GPa), the PVDF nanocomposite ($E = 1.36 \pm 0.04$ GPa), N6 ($E = 1.67 \pm 0.09$ GPa), and the N6 nanocomposite ($E = 2.40 \pm 0.12$ GPa).

**Sequential Compounded Blends with Cloisite 30B.** For the blends in the previous section, the clay nanoparticles were blended with both polymers simultaneously. To better understand the kinetics of nanoparticle diffusion on blend properties, a series of experiments were performed where the 30B clay was first compounded with one polymer and then the resulting composite was compounded with the second polymer. The 30B clay interacts more favorably with N6, so in the blend in which PVDF is blended with 30B first and then with N6 (referred to as (PVDF/30B)/N6), it is expected that 30B will migrate to the interface and/or the matrix. For the inverse sequence blend in which 30B is compounded first with N6 and then with PVDF (referred to as (N6/30B)/PVDF), it is expected that the 30B nanoparticles will more likely reside in the matrix.

To assess the evolution of the clay dispersion, XRD patterns were obtained after the first sequence step and again after the blends were fully compounded (Figure 1c). As expected, 30B compounded with N6 is exfoliated as is the (N6/30B)/PVDF blend. For the inverse sequential blend, 30B compounded only with PVDF is intercalated. When this PVDF/clay composite is compounded with N6, the blend has traces of intercalated clay but appears to be mostly exfoliated. The DSC melting curve of this sequential blend, (PVDF/30B)/N6, confirms the migration of clay from PVDF to N6 as the N6 $\gamma$ crystalline phase, the phase typically present in N6 nanocomposites, is the dominant phase. However the ratio of N6 $\alpha$- to $\gamma$-phase of the (PVDF/30B)/N6 blend is larger than the ratio for the (N6/30B)/PVDF blend, indicating incomplete migration of clay from the PVDF.

TEM images support the overall exfoliation of clay in N6 for both blends (Figure 7). Comparison of the TEM images with each other as well as to the image of the one batch blend (Figure 2b) shows a striking difference among the blends' domain sizes. The PVDF domains in the (PVDF/30B)/N6 blend are ∼110 nm;

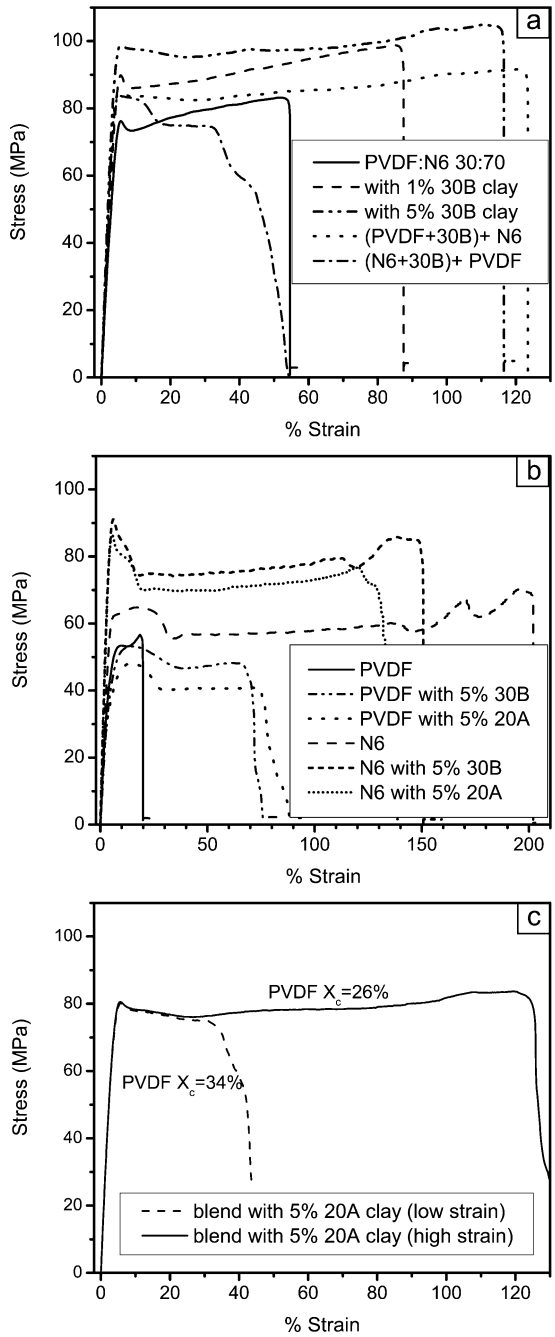


**Figure 6.** Tensile stress−strain curves for (a) blend and 30B modified blends, (b) the homopolymers and their nanocomposites, and (c) 20A modified blend.

the domains are not as small as the one batch blend (~60 nm) but not as large as the domains of the blend with no clay (~150 nm). However, the (N6/30B)/PVDF sequential blend exhibits larger domains (~240 nm) than the blend with no clay. The reasoning for this discrepancy will be addressed in a later section.

In addition to different domain sizes, the amount of PVDF crystallization in the two sequential blends is also different. Unlike the one batch blend with 5% 30B, the PVDF in the sequential blends experiences little or no crystallization suppression. PVDF in the (PVDF/clay)/N6 blend is 24% crystalline, and it is 33% crystalline in the (N6/clay)/PVDF blend. Comparison of the domain size to the PVDF percent crystallinity indicates that smaller domains correlate to less crystalline domains.

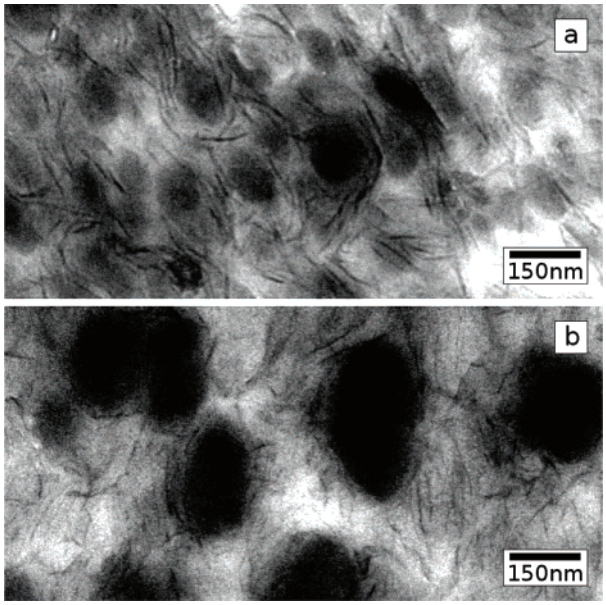


**Figure 7.** TEM micrographs of PVDF/N6 30:70 blend nanocomposites with 5% 30B in which (a) clay was compounded first with PVDF [(PVDF/30B)/N6] and (b) clay was compounded first with N6 [(N6/30B)/PVDF].

Because of the larger domain size and lack of crystallization suppression in the sequence blends, the mechanical properties of the sequential blends were poorer than those of the one batch blend (Figure 6a). The (N6/clay)/PVDF sequence blend with large domains is stiff ($E = 2.52 \pm 0.06$ GPa) but showed no improvement in toughness or strength compared to the blend with no clay. Conversely, the (PVDF/clay)/N6 blend is stiffer ($E = 2.59 \pm 0.04$ GPa), stronger, and tougher compared to the blend with no clay but was inferior to the one batch 30B blend.

**One Batch Blend with 20A.** While the 30B clay interacts favorably with both polymers, it prefers more the N6 and hence is more likely to be dispersed in the matrix. To study the effect of clay location on the blend, a less polar clay, 20A, was chosen for blending. The 20A particles interact comparably with the polymers and are more likely to reside at the interface than the 30B particles.

The blend nanocomposite of PVDF/N6 30:70 with 20A clay shows an intercalated structure (Figure 1b). Since both polymers intercalate to approximately the same *d*-spacing, it cannot be distinguished which one is intercalating the clay. The DSC curve of the blend (Figure 4c) shows both a shift of PVDF melting to higher temperatures and a shift of N6 melting to predominantly $\gamma$-phase, indicating that both polymers are interacting with the clay. It is possible that they both intercalate the clay but not in the same gallery.[8]

TEM images of the blend nanocomposite with 20A clay indicate that the intercalated clay layers are located primarily at the interface interacting with both PVDF and N6 (Figure 8). The images also show the average size of the PVDF domains as being ~120 nm, but unlike the 30B blends, the PVDF domain size for the 20A blend is highly varied ranging from 70 to 150 nm.

The inhomogeneity of domain sizes translated to differing toughness for the 20A blend nanocomposites (Figure 6c). Some blend samples strain hardened and were comparable in elongation to the 30B samples. Other samples failed to strain harden and fractured prematurely, and some fractured somewhere in between. There was not enough statistical consistency despite efforts to improve the processing conditions. Since there was a

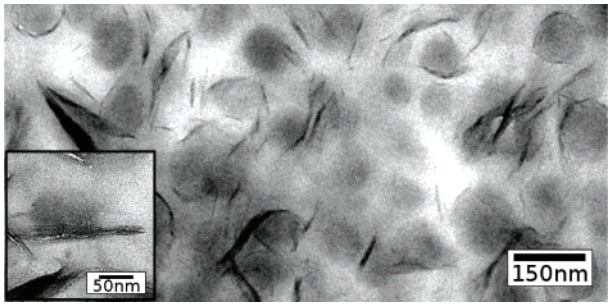


**Figure 8.** TEM micrograph of PVDF/N6 30:70 blend with 5% 20A. Inset shows an intercalated clay structure at the PVDF/N6 interface.

correlation between PVDF crystallinity and toughness in 30B-based nanocomposite blends, DSC measurements were performed on the 20A dog bone specimens at the point of fracture to assess the crystallinity. Indeed, PVDF in high strain fractured samples was ~25% less crystalline than the PVDF in samples that fractured early, reinforcing the idea that crystallization suppression of PVDF is vital to blend toughening. Compare the PVDF percent crystallinity of the low-strain 20A blend ($X_c$ = 34%) and the high-strain 20A blend ($X_c$ = 26%) to the blend with no clay ($X_c$ = 29%) and the sequential blend nanocomposites [$X_c$ = 24% for (PVDF/30B)/N6 and $X_c$ = 33 % for (N6/30B)/PVDF].

## Discussion

The blend nanocomposite that displayed the best compatibilization characteristics is the one batch blend with 5% 30B. In this nanocomposite, the clay prevented the coalescence of the minor phase, stabilized the domain morphology, changed the interfacial properties, and enhanced the blend performance. To some degree these properties were also observed in the (PVDF/30B)/N6 sequence blend and to a lesser extent the blend with 20A. The differences in behavior of these blends offer insight into the overall compatibilization mechanism.

There appears to be a direct link between mechanical toughening and percent crystallinity of the domain phase; tougher blends have less crystalline PVDF domains. The one batch 5% 30B blend was the most tough, and the (PVDF/30B)/N6 sequence blend and 20A blend samples with suppressed crystallinity in the tensile region also displayed large strains to failure. On the other hand, the (N6/30B)/PVDF sequence blend nanocomposite and the 20A blend samples with no crystallinity suppression were less tough.

Controlling the domain size is crucial as the amount of crystallinity scales with domain size. In a polymer blend, which is essentially a mix of two viscous, incompressible fluids, domain size is related to the breakup of threads (surrounded by matrix) into droplets due to Rayleigh instability.[23] Empirically, domain size ($A_n$) has been determined to depend on the interfacial tension ($\gamma$), the viscosity ratio of the dispersed phase to the matrix phase ($\eta_d/\eta_m$), the shear rate ($G$), and the melt viscosity ($\eta_{me}$) as shown in the following equation.[24]

$$A_n = \frac{4\left(\frac{\eta_d}{\eta_m}\right)^k \gamma}{G\eta_{me}} \quad (1)$$

where $k = 0.84$ for $\eta_d/\eta_m \geq 1$ and $k = -0.84$ for $\eta_d/\eta_m \leq 1$. The equation implies (and other experimental studies have shown[25]) that the smallest domains are generally the result of a viscosity ratio that is close to unity. For the blends studied in this work where PVDF is the domain phase and N6 is the matrix phase, the viscosity ratio is less than unity.[1]

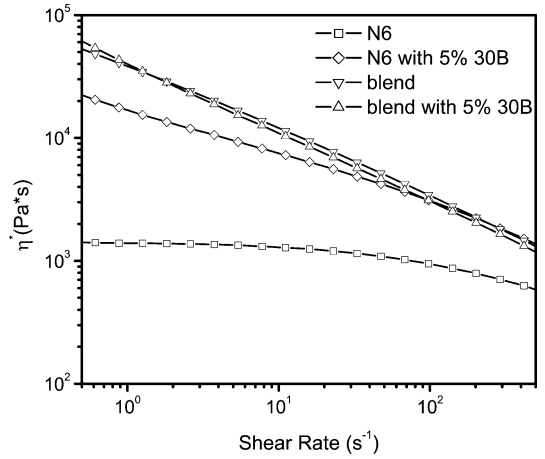


**Figure 9.** Complex viscosity of N6, blend (PVDF:N6 30:70), N6 with 5% 30B, and blend with 5% 30B.

For the blends in the current study, the shear rate ($G$) is held constant as the blends are all extruded at the same rate. The viscosity of the blend melt and the blend with 5% 30B melt are also roughly equal (Figure 9); thus, the only variables that change with the addition of clay are the viscosity ratio and the interfacial tension. In the (N6/30B)/PVDF sequence blend, it is mainly the viscosity of the N6 matrix phase that is affected because the clay is first mixed with N6 and clay migration from N6 to PVDF is exceedingly slow due to the strong interaction between N6 and 30B. At the extrusion temperature, N6 with 5% 30B is 10 times more viscous than pure N6 in the shear rate range of the extruder. Therefore, in the (N6/30B)/PVDF blend, the viscosity ratio effects ($\eta_d/\eta \ll 1$) outweigh any changes in the interfacial tension, resulting in domains that are larger than the blend with no clay (phase coarsening). However, in the one batch 30B and (PVDF/30B)/N6 blends, the interfacial tension is lowered significantly due to the presence of clay at the PVDF−N6 interface. Even though the viscosity of N6 matrix is still increased in these samples (since 30B is exfoliated in N6), the interfacial tension effects seem to outweigh the viscosity effect, resulting in smaller domains for these blends. In the 20A blend nanocomposite, the viscosities for both PVDF and N6 are likely increased as the clay is mostly located at the interface and is probably intercalated by both polymers. If the viscosities of both the matrix and dispersed phases are increased, the viscosity ratio is not as affected by the addition of clay. Thus, in the 20A blend nanocomposite, the interfacial tension effect also seems to outweigh the viscosity effect.

Clay dispersion not only affects the viscosity and interfacial tension (and thus indirectly contributes to the mechanical properties), it also directly influences the mechanical properties by providing reinforcement. The best properties stem from having the clay well dispersed throughout both the matrix and at the interface. The (PVDF/30B)/N6 sequence blend and 20A blend have good interfacial dispersion, but they suffer from insufficient matrix dispersion. Since the clay was not completely dispersed, both blends were not as strong or stiff as the one batch 30B blends. In addition, the poor dispersion in the 20A samples likely caused the varying domain sizes and premature failure in some samples. Ideally, the compatibilizer nanoparticles should interact favorably with both polymers but prefer the matrix polymer like 30B does with N6.

In the ideal blend nanocomposite, one batch 30B blend, the clay plays two roles which work in tandem to compatibilize

the blend. Well-dispersed clay in the N6 matrix of the blend stiffens and strengthens the blend similarly to the clay in the homopolymer. The clay at the interface reduces the interfacial tension, resulting in smaller domains with suppressed crystallization. The "amorphous" PVDF domains seem to toughen the blends. We suspect that the domains are acting as rubbery particles in rubber-toughened polymers. In particular, the percent composition of PVDF domains (30%), the low $T_g$ of PVDF (−40 °C), the small size of the domains, and the compliant nature of PVDF compared to N6 are consistent with a rubbery phase in rubber-toughened N6.[26,27] Further experiments are underway to further elucidate the strengthening/toughening mechanisms. If this is indeed the case and these concepts can be applied more generally to other polymers, nanoparticle compatibilization could potentially be a new method for toughening brittle polymers.

**Acknowledgment.** This work was supported by Motorola University Partnership in Research Program under the guidance of Andrew Skipor. L. Vo also gratefully acknowledges support from the NSFGRP fellowship. This work made use of the Cornell Center for Materials Research Experimental Facilities. We thank Suren Hayrapetyan for his contribution to the initial stages of this project and Antonios Kelarakis for the rheological measurements. We also thank Spiros Anastasiadis, Haris Retsos, and Alexandre Vermogen for helpful discussions.

## References and Notes

(1) Liu, Z. H.; Marechal, Ph.; Jerome, R. *Polymer* **1998**, *39*, 1779−1785.
(2) Kim, K. J.; Cho, H. W.; Yoon, K. J. *Eur. Polym. J.* **2003**, *39*, 1249−1265.
(3) Mascia, L.; Hashim, K. *Polymer* **1998**, *39*, 369−378.
(4) Priya, L.; Jog, J. P. *J. Polym. Sci., Part B: Polym. Phys.* **2002**, *40*, 1682−1689.
(5) Liu, L.; Qi, Z.; Zhu, X. *J. Appl. Polym. Sci.* **1999**, *71*, 1133−1138.
(6) Ray, S. S.; Pouliot, S.; Bousmina, M.; Utracki, L. A. *Polymer* **2004**, *45*, 8403−8413.
(7) Chow, W. S.; Ishak, Z. A.; Ishiaku, U. S.; Karger-Kocsis, J.; Apostolov, A. A. *J. Appl. Polym. Sci.* **2004**, *91*, 175−189.
(8) Ray, S. S.; Bousmina, M. *Macromol. Rapid Commun.* **2005**, *26*, 450−455.
(9) Si, M.; Araki, T.; Ade, H.; Kilcoyne, A. L. D.; Fisher, R.; Sokolov, J. C.; Rafailovich, M. H. *Macromolecules* **2006**, *39*, 4793−4801.
(10) Li, Y.; Shimizu, H. *Polymer* **2004**, *45*, 7381−7388.
(11) Dharaiya, D. P.; Jana, S. C. *J. Polym. Sci., Part B: Polym. Phys.* **2005**, *43*, 3638−3651.
(12) Gelfer, M. Y.; Song, H. H.; Liu, L.; Hsiao, B. S.; Chu, B.; Rafailovich, M.; Si, M.; Zaitsev, V. *J. Polym. Sci., Part B: Polym. Phys.* **2003**, *41*, 44−54.
(13) Voulgaris, D.; Petridis, D. *Polymer* **2002**, *43*, 2213−2218.
(14) Gahleitner, M.; Kretzschmar, B.; Pospiech, D.; Ingolic, E.; Reichelt, N.; Bernreitner, K. *J. Appl. Polym. Sci.*. **2006**, *100*, 283−291.
(15) Ji, G.; Clement, F.; Giannelis, E. P. *MRS Proc.* **2001**, *661*, KK10.1.1.
(16) Tjong, S. C.; Bao, S. P. *J. Polym. Sci., Part B: Polym. Phys.* **2004**, *42*, 2878−2891.
(17) Devaux, E.; Bourbigot. S.; Achari, A. E. *J. Appl. Polym. Sci.* **2002**, *86*, 2416−2423.
(18) Dillion, D. R.; Tenneti, K. K.; Li, C. Y.; Ko, F. R.; Sics, I.; Hsiao, B. S. *Polymer* **2006**, *47*, 1678−1688.
(19) Nakajima, H.; Yamada, K.; Iseki, Y.; Hosoda, S.; Hanai, A.; Oumi, Y.; Teranishi, T.; Sano, T. *J. Polym. Sci., Part B: Polym. Phys.* **2003**, *41*, 3324−3332.
(20) Jiang, S.; Qiao, C.; Tian, S.; Xiangling, J.; An, L.; Jiang, B. *Polymer* **2001**, *42*, 5755−5761.
(21) Strawhecker, K. E.; Manias, E. *Chem. Mater.* **2000**, *12*, 2943−2949.
(22) Vaia, R. A.; Sauer, B. B.; Tse, O. K.; Giannelis, E. P. *J. Polym. Sci., Part B: Polym. Phys.* **1997**, *35*, 59−67.
(23) Palierne, J. F.; Lequeux, F. *J. Non-Newtonian Fluid Mech.* **1991**, *40*, 389−306.
(24) Wu, S. *Polym. Eng. Sci.* **1987**, *27*, 335−343.
(25) Favis, B. D. In *Polymer Blends*; Paul, D. R., Bucknall, C. B., Eds.; John Wiley: New York, 1999; Vol. 1, pp 501−537.
(26) Kudva, R. A.; Keskkula, H.; Paul, D. R. *Polymer* **2000**, *41*, 225−237.
(27) Okada, O.; Keskkula, H.; Paul, D. R. *J. Polym. Sci., Part B: Polym. Phys.* **2004**, *42*, 1739−1758.

MA071508Q